OPTICA

Scalable, fiber-compatible lithium-niobate-on-insulator micro-waveguides for efficient nonlinear photonics

Yuting Zhang,[1,†] Hao Li,[1,†] Tingting Ding,[2,†] Yiwen Huang,[1] Longyue Liang,[1] Xuerui Sun,[1] Yongzhi Tang,[1] Jiayu Wang,[1] Shijie Liu,[1] Yuanlin Zheng,[1,3,*] and Xianfeng Chen[1,3,4,5]

[1]State Key Laboratory of Advanced Optical Communication Systems and Networks, School of Physics and Astronomy, Shanghai Jiao Tong University, Shanghai 200240, China
[2]School of Electronic and Electrical Engineering, Shanghai University of Engineering Science, Shanghai 201620, China
[3]Shanghai Research Center for Quantum Sciences, Shanghai 201315, China
[4]Collaborative Innovation Center of Light Manipulations and Applications, Shandong Normal University, Jinan 250358, China
[5]xfchen@sjtu.edu.cn
[†]These authors contributed equally to this work.
*ylzheng@sjtu.edu.cn

Received 6 March 2023; revised 13 May 2023; accepted 16 May 2023; published 31 May 2023

Efficient wave mixers based on lithium-niobate-on-insulator (LNOI) hold great potential for next-generation photonic integrated circuits in both classical and quantum optics. However, achieving high-performance nonlinear photonic devices readily suitable for scalable, fiber-compatible applications remains challenging. Here, we report on the fabrication of LNOI micrometer waveguides, i.e., micro-waveguides, with a combination of ultraviolet lithography and deep dry etching technology for efficient nonlinear photonics applications. We fabricate periodically poled LNOI micro-waveguides with a cross section of ∼3 × 4 μm^2 and demonstrate a fiber–chip–fiber second-harmonic generation conversion efficiency of 1320%/W with an insertion loss of 3.8 dB at the telecommunication band. We also demonstrate high-quality photon pair generation via spontaneous parametric downconversion with a flux of 178 MHz/mW at sub-mW pump power and coincidence-to-accidental ratio >8000 at microwatt pump power. The overall performance in both applications is on par with that of state-of-the-art counterparts using thin-film lithium niobate nano-waveguides. The technique would make micrometer-thick LNOI an attractive platform for ready applications in nonlinear and quantum optics.

https://doi.org/10.1364/OPTICA.489383

1. INTRODUCTION

Efficient nonlinear wave mixing based on second-order nonlinearity ($\chi^{(2)}$) is significantly important in classical and quantum photonics, where high performance, scalable fabrication capability, and compatibility with fiber are core figures of merit for such kinds of devices in terms of realistic applications. Among all quadratic materials, lithium-niobate-on-insulator (LNOI) is one of the best, which has become the focus of substantial interest and has witnessed exponential growth in photonics based on the novel platform [1–8]. The platform is highly favored due to the exceptional properties of lithium niobate (LN) and a high refractive index contrast ($\Delta n \sim 0.7$ for LN versus SiO_2). These features are highly valuable for efficient nonlinear wave mixing in photonic integrated circuits in various classical and quantum photonics applications. A variety of nonlinear photonic devices have been demonstrated on both micrometer- and nanometer-thick LN films [9–13], with normalized efficiency far superior to conventional proton exchange or Ti indiffused LN waveguides.

Other than high performance, scalable fabrication capability and compatibility with fiber are also considerably important. Current mainstream methods for nano-waveguide fabrication on thin-film LN (TFLN) include inductively coupled plasma (ICP) etching (or dry etching) [14] and chemical mechanical polishing (CMP) [15]. Light is strongly confined in TFLN nano-waveguides for enhanced nonlinearity. Ultra-efficient frequency converters and ultrabright single-photon sources have been demonstrated [10,16–18]. But light coupling into and out of the nano-waveguide can be a big issue. The low fiber-to-chip coupling efficiency because of a huge mode mismatch and small alignment tolerance becomes an obstruction to practical applications, although this can be improved by introducing high-demanding components such as coupling gratings, multi-layer tapered edge couplers, or spot size converters (SSCs) [19–23]. In comparison, micrometer-thick LNOI seems to be more suitable for ready applications in fiber-compatible systems [24–26]. But the fabrication technique was basically limited to high-precision optical grade dicing [27]. The typical thickness of LNOI is 5 μm or greater.

Because mechanical dicing, however precise, exerts a force against the fragile film during the fabrication process, the LN film can easily be cracked during dicing. The normalized conversion efficiency of the nonlinear ridge waveguide is similar to that of conventional ones, as the dimension of the waveguide is similarly large. Also, the mechanical fabrication method has low throughput and moderate reproducibility, which is not ideal for realistic applications either.

There have been few reports on photonics on LNOI whose thickness lies in between, e.g., 3-μm-thick LNOI. The reason that it is considerably valuable is that light coupling with such micro-waveguides can be efficiently high with single-mode lensed fiber or high-numerical-aperture fiber without additional treatment. This is an advantage for practical applications where coupling loss reduction is highly required as in quantum optics. In addition, the required submicrometer precision fabrication is compatible and cost effective for mass fabrication and production. Wafer-scale ultraviolet (UV) lithography becomes readily applicable. The mode area in such LNOI micro-waveguides is still one order of magnitude smaller than that in conventional LN waveguides. Better alignment tolerance also enables easy device packaging. The overall fiber–chip–fiber performance can be well traded off. Although 3-μm-thick LNOI shows plenty of advantages, the current fabrication techniques are not directly applicable. Further efforts are needed to demonstrate scalable fabrication and efficient nonlinear devices on the platform.

Here, we propose and demonstrate fabrication of micro-waveguides on the 3-μm-thick LNOI platform with UV lithography and deep dry etching for efficient nonlinear photonics. Unlike previous works, the approach circumvents most of the existing difficulties and shortcomings, while preserving sufficiently high device performance. We successfully fabricate periodically poled LNOI (PPLNOI) micro-waveguides and show efficient second-harmonic generation (SHG) at the telecommunication band with a normalized conversion efficiency reaching 219%/(W · cm^2). The fiber–chip–fiber conversion efficiency of the 25-mm-long waveguide reaches over 1, 320%/W with an insertion loss of 3.8 dB without anti-reflection coating. We also demonstrate high-quality photon pair generation via spontaneous parametric downconversion (SPDC) with a flux of 178 MHz/mW at a sub-milliwatt pump power and coincidence-to-accidental ratio (CAR) of >8000 at a low pump power of 4 μW. The device performance in both applications is comparable to that of state-of-the-art counterparts using TFLN nano-waveguides. The simple fabrication procedures would also boost large-scale fabrication and promote the development of photonic devices on the LNOI platform.

2. LNOI MICRO-WAVEGUIDE FABRICATION AND CHARACTERIZATION

The fabrication process of LNOI micro-waveguides mainly involves UV lithography and deep dry etching (i.e., ICP with micrometer etch depth) (see Supplement 1 for details). LNOI wafers (NANOLN) consisting of 3-μm-thick z-cut congruent LN film on a 2-μm-thick silica buried layer on top of a silicon substrate are used. First, standard UV lithography is performed to define the periodic electrode pattern followed by a lift-off process. Then the wafer is periodically poled to get the PPLNOI sample. At the second stage, an 8-μm-thick photoresist is spin-coated to define the waveguide mask by UV lithography. The micro-waveguide width is defined accordingly. Thick photoresist is used to withstand the deep dry etching. The following ICP etching transfers the photoresist pattern to the LNOI film. The parameters of argon-ion milling are carefully optimized to control the etching rate and guarantee the sidewall smoothness and etching selectivity [28–30]. In our experiment, 600-W ICP power and 300-W RIE power are applied with an argon gas flow of 40 sccm. The achieved etching rate is 70 nm/min, and the etching selectivity is about 1:1. The obtained sidewall angle is ∼65°. For the 3 μm-thick LNOI, an etching depth of over 2 μm is typically needed to form low-propagation-loss waveguides. Finally, the residual photoresist and etching redeposition are cleaned. PPLNOI micro-waveguides are therefore obtained.

In our experiment, a type-0 quasi-phase matching (QPM) scheme is implemented to utilize the largest nonlinear coefficient, d_{33}, for efficient frequency conversion. The design of the PPLNOI waveguide geometry and the poling period is based on the realization of the first-order QPM condition. The poling pattern can be directly observed in an optical microscope, as shown in Fig. 1(a), which proves high poling quality and uniformity. The achieved poling period is 13.7 μm with a duty cycle of ∼60%, corresponding to first-order QPM in the telecommunication band. The length of our PPLNOI ridge waveguides, as well as the poling section, is 25 mm. Figure 1(b) displays the scanning electron microscope (SEM) image of the end facet of one fabricated micro-waveguide. The micro-waveguide has a cross section of ∼3 × 4 μm^2 and the etching depth is 2.5 μm. Smooth and reproducible etching is achieved using the purely physical method of argon-ion milling. Figures 1(c) shows the numerically simulated optical mode profiles of fundamental transverse magnetic (TM) mode of the fundamental harmonic (FH) at 1578 nm and second harmonic (SH) at 789 nm in the micro-waveguide, which are the experimentally observed QPM wavelengths. The calculated modal effective areas, A_{eff}, are 6.11 μm^2 and 5.71 μm^2, respectively. The normalized mode overlap factor is calculated to be close to unity (∼0.99). It should be noted that the micro-waveguide also supports higher-order modes. Figure 1(d) shows the calculated QPM period with respect to the FH wavelength, indicating a poling period of 13.70 μm for SHG at 1555 nm. This is mainly due to the inevitable error in precisely determining the effective refractive index of the waveguide. The discrepancy between the predicted and observed QPM wavelengths is still quite acceptable. The period is shorter than that in traditional PPLN waveguides but is still quite large, which facilitates the poling procedure. The theoretical normalized SHG conversation efficiency is also plotted in Fig. 1(d), showing that the micro-waveguide lies in between conventional LN and TFLN waveguides. This is principally determined by the dimension of the waveguide, or equivalently, the effective mode area of light in the waveguide.

The waveguide end facets are finely polished but not anti-reflection coated in our devices. The propagation loss of the PPLNOI ridge waveguide is evaluated by the Fabry–Perot (FP) interferometric method [31]. Propagation loss α can be extracted from the transmission (or reflection) spectrum while finely scanning the FH wavelength, i.e., FP interference fringes; see Supplement 1. The propagation loss is evaluated to be 0.3 dB/cm for TE mode and 0.5 dB/cm for TM mode. Slightly larger loss for TM polarization may result from larger sidewall scattering. The fiber–chip–fiber loss is experimentally measured to be 2.9 dB for TE input and 3.8 dB for TM input. This includes the reflection loss

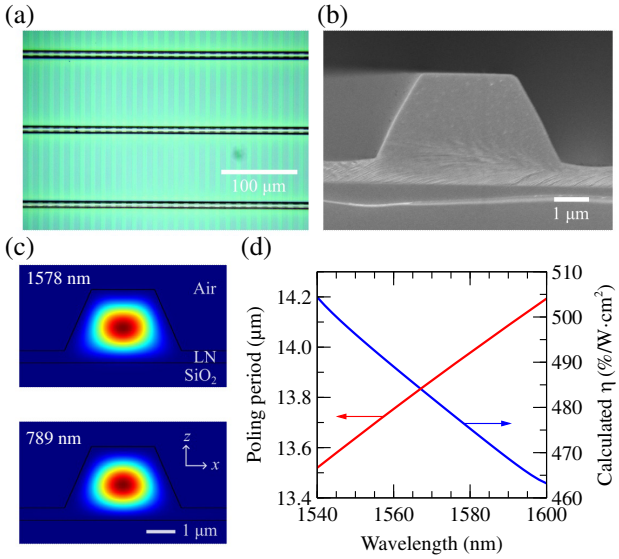

Fig. 1. (a) Microscopy view of the micro-waveguides and periodic poled domains. (b) SEM image of the end facet of the PPLNOI ridge waveguide by cracking the chip. The white line under the waveguide is the crack of the SiO_2 buffering layer. (c) Calculated mode profiles of fundamental TM modes at the 1578-nm and 789-nm wavelengths. (d) Numerically calculated QPM period and theoretical normalized conversion efficiency (η) as a function of the FH wavelength.

at uncoated endfaces, coupling loss between fiber and the micro-waveguide, and intrinsic waveguide propagation loss. This is good enough for most applications. Considering the actual propagation loss, the fiber-waveguide coupling loss is about 1 dB/facet.

3. RESULTS AND DISCUSSION

The performance of the fabricated PPLNOI micro-waveguide device is evaluated via the processes of SHG and SPDC, which are two typical applications in classical and quantum applications, respectively. In our experiment (see Supplement 1 for details), light is coupled into and out of the PPLNOI micro-waveguide using a pair of lensed fibers. To characterize the fiber–chip–fiber performance of the device, light power is measured at the input and output coupling fiber port.

We measure SHG efficiency in the small-signal approximation. Figure 2(a) shows the obtained QPM SHG tuning curve using a continuous wave (cw) laser. The QPM central wavelength is experimentally measured to be 1578.3 nm. We measure the dependence of SH power versus FH power at the QPM wavelength as displayed in Fig. 2(b). A high slope efficiency of $1320 \pm 20\%/\mathrm{W}$ is extracted from the fitting. Such a high fiber–chip–fiber conversion efficiency is the first, to the best of our knowledge, achieved in micro-scale LNOI ridge waveguides. The inset of Fig. 2(b) shows the FH and SH spots at the waveguide output facet, showing they are formed in fundamental spatial modes. It should be noticed that the micro-waveguide supports higher-order spatial modes. The excited fundamental spatial FH mode is determined by the maximum mode overlapping of it with the input fiber mode, and the generated fundamental spatial SH mode is determined by the phase-matching condition and the maximum mode overlapping of it with the fundamental spatial FH mode. Therefore, the generated SH can be efficiently collected by the second lensed fiber.

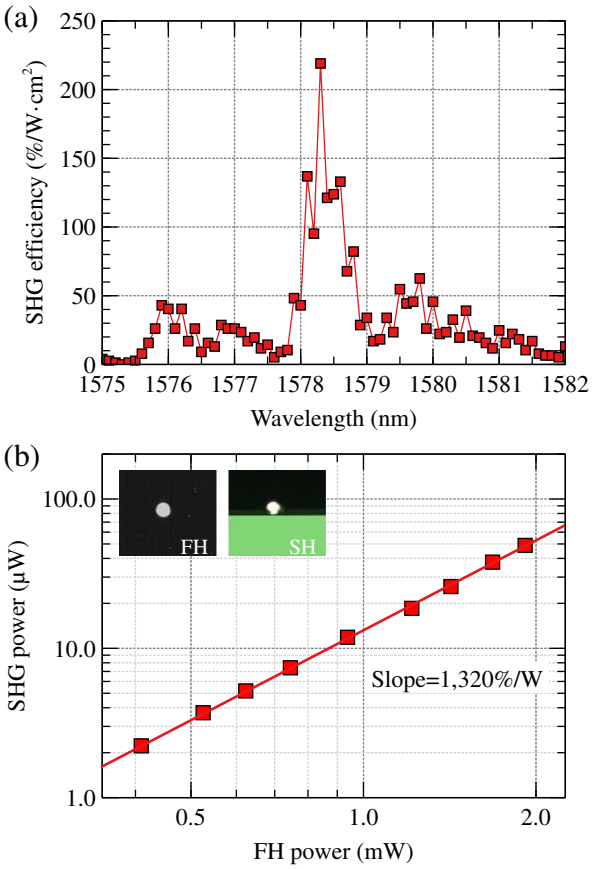

Fig. 2. (a) Measured normalized conversion efficiency (η) versus pump wavelength. (b) Square dependence of SH versus FH power plotted in log–log scale. Inset: FH and SH spots at the output.

For SHG, the normalized conversion efficiency η is defined as $P_{\mathrm{SH}}/(P_{\mathrm{FH}}^2 \cdot L^2)$, where P refers to the power value measured at the out-coupling fiber, and L is the length of the waveguide. The measured normalized conversion efficiency is $219\%/\mathrm{W} \cdot \mathrm{cm}^2$ at small signals, and the theoretical prediction is $476\%/\mathrm{W} \cdot \mathrm{cm}^2$. This value is multiple times greater than that in conventional LN waveguides, but one order of magnitude smaller than that of TFLN nano-waveguides. There is much room to further improve the normalized conversion efficiency (the currently obtained value is only half of the theoretical prediction). This discrepancy mainly attributes to the device loss (including propagation loss and coupling loss) and deviated poling duty from 50%. However, the fiber–chip–fiber conversion efficiency of our PPLNOI micro-waveguide still reaches up to 1320%/W. Benefiting from better mode confinement by decreasing the cross-sectional area and improved coupling efficiency, the normalized and absolute conversion efficiencies are increased as compared with large-core LNOI ridge waveguides and TFLN nano-waveguides, respectively; see also Table 1 in Supplement 1. Our scheme benefits the applications of LNOI ridge waveguides for frequency converters and quantum sources.

Compared with state-of-the-art frequency converters based on LNOI ridge waveguides or TFLN nano-waveguides [10,24–26,32–34], our PPLNOI device has the best comprehensive performance, which well balances the trade-off among normalized efficiency, coupling efficiency, and device length. This is important for ready applications in nonlinear photonics. Efficient conversion in LNOI micro-waveguides would also promote other

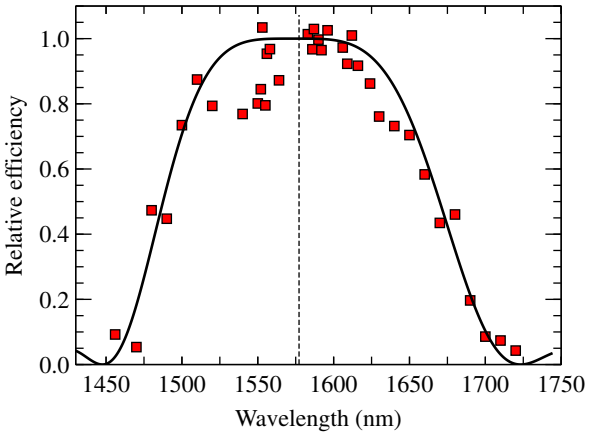

Fig. 3. Spectrum of SPDC in the PPLNOI micro-waveguide pumped at 789 nm.

applications such as sum-frequency generation (e.g., for NIR or single-photon upconversion detection), difference frequency generation (e.g., for wavelength conversion or quantum interfaces), as well as optical parametric amplification (e.g., for microwave photonics). Especially, for important applications in the IR or terahertz regime, e.g., "fingerprint" gas detection and terahertz generation, micro-waveguides would also be more suitable than nano-waveguides.

Moreover, the PPLNOI micro-waveguide can be used for efficient generation of photon pairs or herald single photons via QPM SPDC. A reduced modal area not only lowers the power requirement but also improves the quality of the generated photon pairs. Traditional LN waveguides are relatively inefficient, and TFLN nano-waveguides encounter large direct coupling loss. They typically require milliwatt and sub-milliwatt power laser pumps. Efficient single-photon sources at microwatt power in the telecommunication band are under active study and highly desirable in quantum networks, where our scheme provides a ready solution.

First, we investigate the quantum source in terms of the downconverted biphoton spectrum. A tunable filter with a full-width-at-half-maximum (FWHM) bandwidth of 0.5 nm is utilized. In the measurement, we scan the tunable grating filter and record the time-averaged value of the detected photon rate at different wavelengths with an acquisition time of 10 s. Figure 3 shows the experimental spectrum of the generated SPDC photons from the PPLNOI micro-waveguide recording at the out-coupling fiber. The spectrum of the photon pairs is symmetric with respect to the central wavelength of 1578 nm and manifests strong frequency correlation due to the energy conservation of the parametric process. The FWHM spectrum spans a range of approximately 200 nm, covering the whole telecom S-, C- and L-bands. The weak dispersion property of the PPLN in the telecommunication band and high efficiency of the nonlinear process allow the SPDC photons to populate such a large number of frequency modes.

Next, we measure the brightness of our device to further characterize the high-flux source, which is one of the most important resources for quantum information applications. To investigate the pair flux, the photon pair generation rate (PGR) is experimentally obtained by integrating the time-averaged coincidence count histogram. During the measurement, a 100-GHz dense wavelength division multiplexer (DWDM) filter is used to divide the SPDC photons. Figure 4(a) shows the measured photon PGR

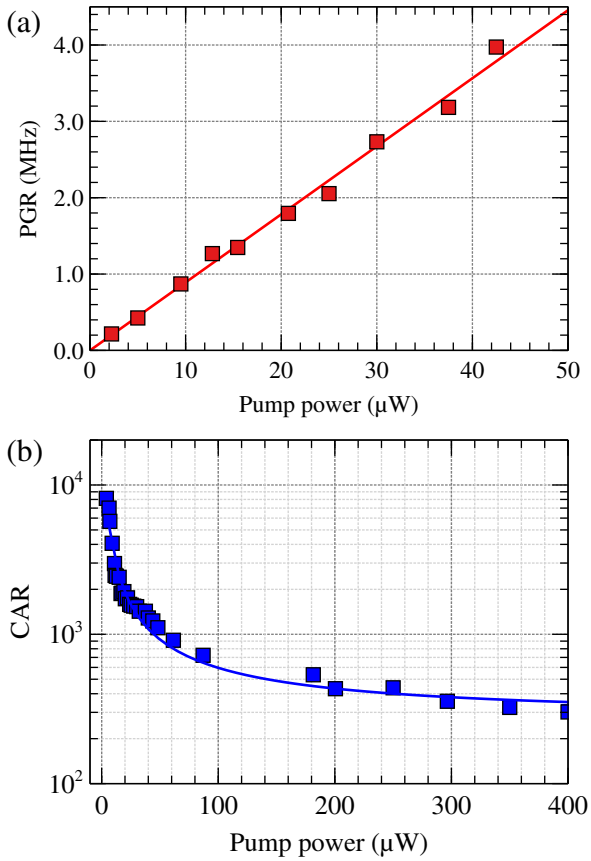

Fig. 4. (a) PGR and (b) CAR measurement versus pump power in the PPLNOI micro-waveguide.

for different input pump powers at the out-coupling fiber, which takes the transmission of the filters and the detector efficiencies into account. The data fit cleanly into a linear line owing to the PGR changing linearly with the pump power, and the generation efficiency can be evaluated as the slope of the line. The highest PGR counting is limited only by the superconducting nanowire single photon detector (SNSPD). The fitting result of the experimental data has a slope of 89 MHz/mW. The device has a 6-dB insertion loss for the 789-nm pump. The corresponding value at the output facet of the micro-waveguide is 178 MHz/mW. Both are higher than that of the traditional PPLN waveguide and TFLN waveguide. The brightness of the SPDC source of our device is 9.0×10^7 pairs s^{-1} nm^{-1} mW^{-1} at the output fiber or 1.8×10^8 pairs s^{-1} nm^{-1} mW^{-1} at the waveguide output facet. Considering the FWHM bandwidth of about 200 nm of the SPDC spectrum, we can calculate the flux efficiency to be about 36 GHz/mW, which makes the source promising for broad applications in quantum information applications over fiber networks or on a chip.

To further investigate the performance of the quantum source, we measure the noise characteristics of the source. The CAR factor is the quality merit for characterizing the signal-to-noise ratio of photon pairs. In theory, CAR can be expressed as $\mathrm{CAR} = C\eta_i\eta_s/(C+\eta_i D_s)(C+\eta_s D_i)$, where C is the coincidence rate, and η and D are the detection efficiency and dark count rate of the single-photon detectors, respectively. Subscripts s, i denote signal and idler, respectively. To measure the two-photon cross-correlation, a DWDM filter and two tunable filters with an FWHM bandwidth of 0.1 nm are used to separate the signal and

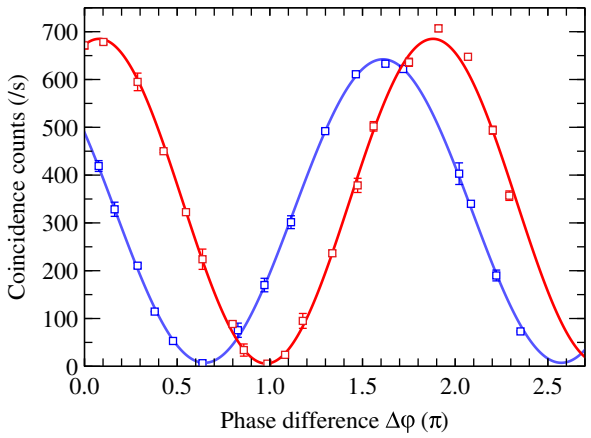

Fig. 5. Measured two-photon interference pattern as the relative phase of the MZI in the signal path is swept.

idler photons in the experiment. Figure 4(b) shows the experimental CAR of the photon pairs under different pump levels. The CAR degrades with pump power due to multi-pair generation events. The highest CAR was 8136 measured at an output flux or PGR of 355 kHz at an input power of 4.0 μW (the corresponding on-chip flux PGR is 710 kHz). At the highest used power of 400 μW, the CAR factor is still greater than 300. The estimated PGR in the output fiber would be 35 MHz as extracted from Fig. 4(a). The product of CAR and PGR in the waveguide is higher than that in TFLN nano-waveguides [17,18]. A higher CAR can be achieved by decreasing the loss of tunable fiber grating filters (∼3 dB in our experiment).

To verify the non-classical property of the quantum source, we characterize the time–energy entanglement of photon pairs. An inherent feature in photon pairs generated via SPDC is characterized by the Franson-type two-photon interference by violating Bell's inequality [35]. In our experiment, we use the Franson-type interferometer, which consists of two 1-GHz unbalanced Mach–Zehnder interferometers (MZIs) to characterize the time–energy entanglement. The two-photon interference patterns under two nonorthogonal phase bases are measured by sweeping the relative phase of the MZI in the signal photon path. The result is shown in Fig. 5. We obtain an average fringe visibility of $V = (98.2 \pm 0.3)\%$, which reveals a high quality of the time–energy entanglement by exceeding the nonlocal bound 70.7% of the Bell inequality [36]. The experimental result confirms the high quality of the time–energy entanglement properties of the generated photon pair. This also proves that our PPLNOI micro-waveguide can serve as a high-quality quantum entangled source and is readily applicable for quantum communication and computing.

An efficient nonlinear device on the 3 μm LNOI platform can be produced economically and at scale by our proposed method of UV lithography and deep dry etching. The performance of the device can be improved with further reduced propagation loss, waveguide uniformity, anti-reflection coating, and optimized fiber coupling, which is technically feasible in the future. In addition, with magnesium-oxide or zinc-oxide doping, MgO:LNOI or ZnO:LNOI waveguides are capable of handling high-power lasers, even on the several watts level. Our work demonstrates the significant potential of LNOI micro-waveguides for efficient nonlinear and quantum optics applications. Ready application in fiber-compatible networks can be expected in the short future as mass-scale fabrication and low coupling loss become easy and cost effective. We envisage that in the short future, LNOI micro-waveguides could provide a competing platform for a new class of integrated light sources spanning the near to terahertz spectra for classical photonics and high-quality bright single-photon sources for realistic quantum networks.

4. CONCLUSION

In conclusion, we propose and demonstrate UV lithography and deep dry etching to fabricate LNOI micro-waveguides and show their capability in achieving efficient SHG and SPDC. The device well balances the trade-offs in integrated nonlinear photonics implementations. The fiber–chip–fiber performance of our PPLNOI micro-waveguide is better than that of state-of-the-art counterparts using LNOI nano-waveguides. Features of high performance, easy fabrication, and efficient fiber coupling make our devices highly appealing for practical applications. Our work servers as a first step to enable scalable devices on 3-μm-thick LNOI. The advancement would make micrometer-thick LNOI an attractive platform for applications in nonlinear and quantum optics as mass-scale fabrication and low coupling loss become easily accessible and cost effective.

Funding. National Natural Science Foundation of China (12074252, 12192252, 62005159, 62022058); National Key Research and Development Program of China (2022YFA120018801); Shanghai Municipal Science and Technology Major Project (2019SHZDZX01-ZX06); Shanghai Rising-Star Program (20QA1405400); Yangyang Development Fund.

Disclosures. The authors declare no conflicts of interest.

Data availability. Data underlying the results presented in this paper are not publicly available at this time but may be obtained from the authors upon reasonable request.

Supplemental document. See Supplement 1 for supporting content.

REFERENCES

1. A. Boes, B. Corcoran, L. Chang, J. Bowers, and A. Mitchell, "Status and potential of lithium niobate on insulator (LNOI) for photonic integrated circuits," Laser Photon. Rev. **12**, 1700256 (2018).
2. A. Honardoost, K. Abdelsalam, and S. Fathpour, "Rejuvenating a versatile photonic material: thin-film lithium niobate," Laser Photon. Rev. **14**, 2000088 (2020).
3. J. Lin, F. Bo, Y. Cheng, and J. Xu, "Advances in on-chip photonic devices based on lithium niobate on insulator," Photon. Res. **8**, 1910–1936 (2020).
4. A. Boes, L. Chang, C. Langrock, M. Yu, M. Zhang, Q. Lin, M. Lončar, M. Fejer, J. Bowers, and A. Mitchell, "Lithium niobate photonics: unlocking the electromagnetic spectrum," Science **379**, eabj4396 (2023).
5. G. Chen, N. Li, J. D. Ng, H.-L. Lin, Y. Zhou, Y. H. Fu, L. Y. T. Lee, Y. Yu, A.-Q. Liu, and A. J. Danner, "Advances in lithium niobate photonics: development status and perspectives," Adv. Photon. **4**, 034003 (2022).
6. D. Zhu, L. Shao, M. Yu, R. Cheng, B. Desiatov, C. J. Xin, Y. Hu, J. Holzgrafe, S. Ghosh, A. Shams-Ansari, E. Puma, N. Sinclair, C. Reimer, M. Zhang, and M. Lončar, "Integrated photonics on thin-film lithium niobate," Adv. Opt. Photon. **13**, 242–352 (2021).
7. Y. Zheng and X. Chen, "Nonlinear wave mixing in lithium niobate thin film," Adv. Phys. X **6**, 1889402 (2021).
8. S. Saravi, T. Pertsch, and F. Setzpfandt, "Lithium niobate on insulator: an emerging platform for integrated quantum photonics," Adv. Opt. Mater. **9**, 2100789 (2021).
9. D. D. Hickstein, D. R. Carlson, A. Kowligy, M. Kirchner, S. R. Domingue, N. Nader, H. Timmers, A. Lind, G. G. Ycas, M. M. Murnane, H. C. Kapteyn, S. B. Papp, and S. A. Diddams, "High-harmonic generation in periodically poled waveguides," Optica **4**, 1538–1544 (2017).

10. C. Wang, C. Langrock, A. Marandi, M. Jankowski, M. Zhang, B. Desiatov, M. M. Fejer, and M. Lončar, "Ultrahigh-efficiency wavelength conversion in nanophotonic periodically poled lithium niobate waveguides," Optica **5**, 1438–1441 (2018).
11. C. Lu, H. Li, J. Qiu, Y. Zhang, S. Liu, Y. Zheng, and X. Chen, "Second and cascaded harmonic generation of pulsed laser in a lithium niobate on insulator ridge waveguide," Opt. Express **30**, 1381–1387 (2022).
12. J. Lu, J. B. Surya, X. Liu, A. W. Bruch, Z. Gong, Y. Xu, and H. X. Tang, "Periodically poled thin-film lithium niobate microring resonators with a second-harmonic generation efficiency of 250,000%/w," Optica **6**, 1455–1460 (2019).
13. J. Lu, A. A. Sayem, Z. Gong, J. B. Surya, C.-L. Zou, and H. X. Tang, "Ultralow-threshold thin-film lithium niobate optical parametric oscillator," Optica **8**, 539–544 (2021).
14. C. Wang, M. J. Burek, Z. Lin, H. A. Atikian, V. Venkataraman, I.-C. Huang, P. Stark, and M. Lončar, "Integrated high quality factor lithium niobate microdisk resonators," Opt. Express **22**, 30924–30933 (2014).
15. R. Wu, M. Wang, J. Xu, J. Qi, W. Chu, Z. Fang, J. Zhang, J. Zhou, L. Qiao, Z. Chai, J. Lin, and Y. Cheng, "Long low-loss-litium niobate on insulator waveguides with sub-nanometer surface roughness," Nanomaterials **8**, 910 (2018).
16. L. Wang, X. Zhang, and F. Chen, "Efficient second harmonic generation in a reverse-polarization dual-layer crystalline thin film nanophotonic waveguide," Laser Photon. Rev. **15**, 2100409 (2021).
17. J. Zhao, C. Ma, M. Rüsing, and S. Mookherjea, "High quality entangled photon pair generation in periodically poled thin-film lithium niobate waveguides," Phys. Rev. Lett. **124**, 163603 (2020).
18. U. A. Javid, J. Ling, J. Staffa, M. Li, Y. He, and Q. Lin, "Ultrabroadband entangled photons on a nanophotonic chip," Phys. Rev. Lett. **127**, 183601 (2021).
19. S. Kang, R. Zhang, Z. Hao, D. Jia, F. Gao, F. Bo, G. Zhang, and J. Xu, "High-efficiency chirped grating couplers on lithium niobate on insulator," Opt. Lett. **45**, 6651–6654 (2020).
20. B. Chen, Z. Ruan, X. Fan, Z. Wang, J. Liu, C. Li, K. Chen, and L. Liu, "Low-loss fiber grating coupler on thin film lithium niobate platform," APL Photon. **7**, 076103 (2022).
21. L. He, M. Zhang, A. Shams-Ansari, R. Zhu, C. Wang, and L. Marko, "Low-loss fiber-to-chip interface for lithium niobate photonic integrated circuits," Opt. Lett. **44**, 2314–2317 (2019).
22. C. Hu, A. Pan, T. Li, X. Wang, Y. Liu, S. Tao, C. Zeng, and J. Xia, "High-efficient coupler for thin-film lithium niobate waveguide devices," Opt. Express **29**, 5397–5406 (2021).
23. X. Liu, S. Gao, C. Zhang, Y. Pan, R. Ma, X. Zhang, L. Liu, Z. Xie, S. Zhu, S. Yu, and X. Cai, "Ultra-broadband and low-loss edge coupler for highly efficient second harmonic generation in thin-film lithium niobate," Adv. Photon. Nexus **1**, 016001 (2022).
24. T. Umeki, O. Tadanaga, and M. Asobe, "Highly efficient wavelength converter using direct-bonded PPZnLN ridge waveguide," IEEE J. Quantum Electron. **46**, 1206–1213 (2010).
25. C.-W. Hsu, J.-Y. Lai, C.-S. Hsu, Y.-T. Huang, K. Wu, and M.-H. Chou, "Efficient, watt-level frequency doubling and optical parametric amplification on periodically poled lithium niobate ridge waveguide," Proc. SPIE **10902**, 109020D (2019).
26. T. Kazama, T. Umeki, S. Shimizu, T. Kashiwazaki, K. Enbutsu, R. Kasahara, Y. Miyamoto, and K. Watanabe, "Over-30-dB gain and 1-dB noise figure phase-sensitive amplification using a pump-combiner-integrated fiber I/O PPLN module," Opt. Express **29**, 28824–28834 (2021).
27. R. Takigawa, E. Higurashi, T. Kawanishi, and T. Asano, "Lithium niobate ridged waveguides with smooth vertical sidewalls fabricated by an ultraprecision cutting method," Opt. Express **22**, 27733–27738 (2014).
28. Z. Ren, P. J. Heard, J. M. Marshall, P. A. Thomas, and S. Yu, "Etching characteristics of $LiNbO_3$ in reactive ion etching and inductively coupled plasma," J. Appl. Phys. **103**, 034109 (2008).
29. G. Ulliac, V. Calero, A. Ndao, F. Baida, and M.-P. Bernal, "Argon plasma inductively coupled plasma reactive ion etching study for smooth sidewall thin film lithium niobate waveguide application," Opt. Mater. **53**, 1–5 (2016).
30. K. Luke, P. Kharel, C. Reimer, L. He, M. Loncar, and M. Zhang, "Wafer-scale low-loss lithium niobate photonic integrated circuits," Opt. Express **28**, 24452–24458 (2020).
31. R. Regener and W. Sohler, "Loss in low-finesse $Ti:LiNbO_3$ optical waveguide resonators," Appl. Phys. B **36**, 143–147 (1985).
32. A. Rao, K. Abdelsalam, T. Sjaardema, A. Honardoost, G. F. Camacho-Gonzalez, and S. Fathpour, "Actively-monitored periodic-poling in thin-film lithium niobate photonic waveguides with ultrahigh nonlinear conversion efficiency of $4600\%/w^{-1}cm^{-2}$," Opt. Express **27**, 25920–25930 (2019).
33. Y. Niu, C. Lin, X. Liu, Y. Chen, X. Hu, Y. Zhang, X. Cai, Y.-X. Gong, Z. Xie, and S. Zhu, "Optimizing the efficiency of a periodically poled LNOI waveguide using in situ monitoring of the ferroelectric domains," Appl. Phys. Lett. **116**, 101104 (2020).
34. J. Zhao, M. Rüsing, U. A. Javid, J. Ling, M. Li, Q. Lin, and S. Mookherjea, "Shallow-etched thin-film lithium niobate waveguides for highly-efficient second-harmonic generation," Opt. Express **28**, 19669–19682 (2020).
35. P. G. Kwiat, A. M. Steinberg, and R. Y. Chiao, "High-visibility interference in a bell-inequality experiment for energy and time," Phys. Rev. A **47**, R2472–R2475 (1993).
36. J. F. Clauser, M. A. Horne, A. Shimony, and R. A. Holt, "Proposed experiment to test local hidden-variable theories," Phys. Rev. Lett. **23**, 880–884 (1969).